The high frequency response correction of eddy covariance fluxes. Part 1: an experimental approach and its interdependence with the time-lag estimation

Olli Peltola[1], Toprak Aslan[2], Andreas Ibrom[3], Eiko Nemitz[4], Üllar Rannik[2], and Ivan Mammarella[2]

[1]Climate Research Programme, Finnish Meteorological Institute, P.O. Box 503, 00101 Helsinki, Finland
[2]Institute for Atmospheric and Earth System Research (INAR)/Physics, Faculty of Science, University of Helsinki, P.O. Box 68, 00014 Helsinki, Finland
[3]Dept. Environmental Engineering, Technical University of Denmark (DTU), Lyngby, Denmark
[4]UK Centre for Ecology and Hydrology (UKCEH), Edinburgh Research Station, Penicuik, Bush Estate, EH26 0QB, UK

Correspondence: Olli Peltola (olli.peltola@fmi.fi)

Abstract. The eddy covariance (EC) technique has emerged as the prevailing method to observe ecosystem - atmosphere exchange of gases, heat and momentum. EC measurements require rigorous data processing to derive the fluxes that can be used to analyse exchange processes at the ecosystem - atmosphere interface. Here we show that two common post-processing steps (time-lag estimation via cross-covariance maximisation, and correction for limited frequency response of the EC measurement system) are interrelated and this should be accounted for when processing EC gas flux data. These findings are applicable to EC systems employing closed- or enclosed-path gas analysers which can be approximated to be linear first-order sensors. These EC measurement systems act as a low-pass filters on the time-series of the scalar χ (e.g. CO_2, H_2O) and this induces a time-lag (t_{lpf}) between vertical wind speed (w) and scalar χ time series which is additional to the travel time of the gas signal in the sampling line (tube, filters). Time-lag estimation via cross-covariance maximisation inadvertently accounts also for t_{lpf} and hence overestimates the travel time in the sampling line. This results in a phase shift between the time-series of w and χ, which distorts the measured cospectra between w and χ and hence has an effect on the correction for dampening of EC flux signal at high frequencies. This distortion can be described with a transfer function related to the phase shift (H_p) which is typically neglected when processing EC flux data. Based on analyses using EC data from two contrasting measurement sites, we show that the low-pass filtering induced time-lag increases approximately linearly with the time constant of the low-pass filter, and hence the importance of H_p in describing the high frequency flux loss increases as well. Incomplete description of these processes in EC data processing algorithms results in flux biases of up to 10%, with the largest biases observed for short towers due to prevalence of small scale turbulence. Based on these findings, it is suggested that spectral correction methods implemented in EC data processing algorithms are revised to account for the influence of low-pass filtering induced time-lag.

1 Introduction

The eddy covariance (EC) is the standard micrometeorological technique for measuring vertical turbulent fluxes of momentum, heat and gases in the atmospheric surface layer (Aubinet et al., 2012). Under certain conditions (flat terrain, homogeneous and

1

stationarity turbulent flows, source/sink homogeneity, absence of chemical sources/sinks), the measured EC fluxes represent direct and continuous estimates of the surface exchange of energy and matter between the surface and the atmosphere, and are then widely used to estimate energy and water balances, as well as carbon budget of different type of ecosystems (Baldocchi, 2003; Vesala et al., 2008; Mammarella et al., 2015).

Gas flux measurements are made using a three-dimensional sonic anemometer and a gas analyser, which are able to provide fast-response measurements of turbulent fluctuations of vertical wind velocity and gas concentration (Aubinet et al., 2012). All EC systems, including open-path, enclosed-path or closed-path gas analysers, act as low pass filters, and thus cause a systematic bias to flux estimates. Flux loss at high frequency is due to the incapability of the measurement system to detect small-scale variation. The main reasons for co-spectral attenuation are inadequate frequency response of the sensor, sensor separation and line averaging, as well as, in closed-path systems, the sampling of air through tubes and filters.

The frequency response correction is usually performed based on *a priori* knowledge of the system transfer function and the unattenuated cospectrum:

$$CF = \frac{\int_{f_1}^{f_2} Co^{w,\chi} \, df}{\int_{f_1}^{f_2} Co^{w,\chi} H_{lpf} \, df}. \tag{1}$$

Here CF is the estimated spectral correction factor, $Co^{w,\chi}$ the normalised unattenuated cospectrum between scalar (χ) and vertical wind speed (w), f the frequency, H_{lpf} the total transfer function describing the low-pass filtering, and f_1 and f_2 are the integration limits that are determined by the length of the averaging period and Nyquist frequency, respectively. The correction, performed by multiplying the measured covariance by the factor CF, always increases the absolute flux magnitude. Note that the high-pass transfer function (Rannik and Vesala, 1999) is not included in Eq. (1), as here we focus only on the low-pass filtering effect of the EC system. The low-pass filtering transfer function H_{lpf} can be derived either theoretically or empirically (Foken et al., 2012a). The correction is in general different for momentum flux, sensible and latent heat fluxes and the various gas fluxes, and is specific to each EC system. In the theoretical approach, the atmospheric surface layer co-spectral models (Moncrieff et al., 1997) are used, and H_{lpf} is calculated as a convolution of specific transfer functions representing different causes of flux loss, the equations for which can be found in Moncrieff et al. (1997) and Moore (1986). This approach works well for correcting the fluxes of momentum and sensible heat, as well as gas fluxes measured by open-path systems. Further, Horst (1997) and Massman (2000) have proposed alternative theoretical approaches, providing an analytical estimation of correction factors.

Alternatively, the empirical approach can be used, where the model cospectra and H_{lpf} are estimated using in situ measurements. This is the preferable approach for closed-path systems, where additional effects related to the inlet dust filters and rain caps (Aubinet et al., 2016; Metzger et al., 2016), potential variations in the sampling line flow rate, and absortion/desorption processes inside the sampling tube (Ibrom et al., 2007a; Nordbo et al., 2014; Runkle et al., 2012) may contribute to the EC system cut-off frequency, introducing transfer functions which are difficult to estimate *a priori*.

For this approach, different methods have been proposed for retrieving H_{lpf} from the measured power spectra or cospectra of the sonic temperature T and the target gas dry mole fraction (Fratini et al., 2012; Ibrom et al., 2007a; Mammarella et al.,

2009; Nordbo et al., 2014). While the use of power spectra is the method recommended by the ICOS methodology (Sabbatini et al., 2018; Nemitz et al., 2018) and is implemented in the EddyPro software package, other studies and software packages (EddyUH) have supported the use of measured cospectra (Aubinet et al., 2000; Mammarella et al., 2009, 2016) for the empirical retrieval of H_{lpf}. The companion paper (Aslan et al., 2020) has investigated methodological issues and flux uncertainty related

5 to these two methods under different attenuation conditions and signal-to-noise ratio scenarios.

In EC systems, particularly those using closed-path gas analysers, the measurements of vertical wind velocity and gas concentration are not co-located, and a time delay between the two signals exists (Aubinet et al., 2012). The standard procedure is to determine this time delay for each averaging period (typically 30 minutes) by maximising the related cross-covariance function (in absolute terms), and taking the corresponding lag as the true signal delay. However, this time shift between the two

10 signals depends not only on the system setup (e.g. air sample travel time from the inlet to the IRGA sampling cell, separation distance between the inlet and the centre of the sonic anemometer path), but it can additionally reflect the low-pass filtering of the measured signal (Massman, 2000; Ibrom et al., 2007b, a).

In this study, we investigate how the low-pass filtering induced phase shift affects the estimation of the high frequency flux loss, and we show the implications that occur when H_{lpf} time constants are empirically derived from measured power spectra

15 or cospectra, and related CFs values are applied to covariances estimated from the cross-covariance maximum. Finally, we present a method to take the phase shift effect into account when processing EC data. Towards these aims, we use EC data collected above a forest canopy (Hyytiälä) and a wetland (Siikaneva) in Finland covering a large range of attenuation conditions and integral turbulent time scale characteristics.

2 Theory

20 ### 2.1 Transfer functions

The measured cross-spectrum (Cr_m) between the fluctuations of vertical wind speed and the attenuated and lagged scalar can be described by (e.g. Massman (2000)):

$$Cr_m = [Z_w] [h_\chi Z_\chi]^* e^{-j\phi_{phys}}, \tag{2}$$

where Z_w and Z_χ are Fourier transforms of the time series of vertical wind speed (w') and scalar (χ') fluctuations which

25 are perfectly in phase and not attenuated, h_χ is the Fourier transform of the filter function that describes the response of the instrument measuring the scalar time series, $j = \sqrt{-1}$ and $\phi_{phys} = \omega t_{phys}$, where t_{phys} is a constant time shift (s) between w' and χ' and $\omega = 2\pi f$ is the angular frequency, with f representing the frequency (Hz). The superscript * denotes complex conjugation. Equation (2) describes the cross-spectra measured with a typical EC system employing closed-path gas analyser where the scalar fluctuations are attenuated (h_χ), and delayed in time (t_{phys}) with respect to w' due to the gas sampling system

30 (tubes, filters) and horizontal sensor separation. The signal travel time in the gas sampling line (t_{phys}) could be approximated from the volume of the sampling line and flow rate. Note that we assume that the sensor measuring w' is perfect without any

distortions in the measured w' time series. This assumption does not limit the generality of the findings below. We also neglect any influence of sensor separation (Horst and Lenschow, 2009) or high-pass filtering on flux attenuation.

Following, e.g., Horst (1997) and Massman (2000), the scalar sensor is approximated to be a linear first-order sensor for which h_χ can be written as

$$h_\chi = \frac{1}{1 - j\omega\tau}, \tag{3}$$

where τ is the time constant (s) of the filter, also called response time. Note that $Z_w Z_\chi^*$ is the true cross-spectrum (Cr) between unattenuated w' and χ' time series which are in phase and it has a real (cospectrum Co) and an imaginary (quadrature spectrum Q) part ($Cr = Z_w Z_\chi^* = Co + jQ$). Recall also that the integral of Co equals the unattenuated covariance $\overline{w'\chi'}$, i.e. the vertical turbulent flux of scalar χ. Following previous studies (Horst, 1997; Massman, 2000), the quadrature spectrum (Q) can be assumed to be zero for stationary turbulent flow and hence $Cr = Z_w Z_\chi^* \approx Co$. Now, using Euler's formula and some derivation (see Appendix A), we find

$$Cr_m = \frac{\cos\phi_{phys} - \omega\tau\sin\phi_{phys}}{1 + \omega^2\tau^2}Co - j\frac{\sin\phi_{phys} + \omega\tau\cos\phi_{phys}}{1 + \omega^2\tau^2}Co = Co_m + jQ_m, \tag{4}$$

where the first term on the right equals the measured cospectrum (Co_m) and the second term the measured quadrature spectrum (Q_m). Note that whilst Q was assumed to be negligible, Q_m is in fact not equivalent to zero even when $\phi_{phys} = 0$, i.e. when the travel time of scalar χ' signal in the sampling system is zero. This means that w' and the attenuated $\hat{\chi}'$ (^denotes attenuation throughout the text), depending on frequency, can be out of phase due to low-pass filtering of Z_χ with h_χ. This has already previously been noted (e.g. Massman, 2000; Massman and Lee, 2002; Wintjen et al., 2020). Now, simply based on the real part of Cr_m, we can define a transfer function for the first-order system (H) as

$$H = \frac{1}{1 + \omega^2\tau^2}, \tag{5}$$

and a transfer function (H_p) for a generic phase shift ϕ as (Massman, 2000):

$$H_p = \cos\phi - \omega\tau\sin\phi. \tag{6}$$

These two transfer functions together describe how the measured cospectrum (Co_m) deviates from the cospectrum calculated from ideal measurements free from any attenuation and time shifts (Co).

Similarly, forming the cross-spectrum of the attenuated scalar with itself yields:

$$Cr_{m,p} = [h_\chi Z_\chi][h_\chi Z_\chi]^* \tag{7}$$

$$= \frac{1}{1 + \omega^2\tau^2}Z_\chi Z_\chi^* = H Z_\chi Z_\chi^*, \tag{8}$$

where $Z_\chi Z_\chi^*$ is the unattenuated power spectrum. From this it follows that the same transfer function (i.e. H) applies to both power spectrum and cospectrum in the case that there is no phase shift between w' and χ' (i.e. H_p equals 1) and the quadrature spectrum Q is zero.

2.2 Time lag determination via cross-covariance maximisation

Ideally the time lag between w' and $\hat{\chi}'$ would be estimated from the known dimensions of the gas sampling system and flow rate, in addition to other components causing time delay between signals. However, it is in practise difficult to keep track of all the components causing the time delay and hence a practical (yet sometimes flawed (e.g. Langford et al., 2015)) solution has been to estimate the time lag between w' and $\hat{\chi}'$ via cross-covariance maximisation. This can be considered to be equivalent to finding a time shift t (and hence $\phi = \omega t$) that maximises the integral of Co_m above (i.e. maximises the covariance between w' and $\hat{\chi}'$):

$$\int_0^{\infty} \frac{\cos(\omega t) - \omega \tau \sin(\omega t)}{1 + \omega^2 \tau^2} Co\, d\omega = \overline{w'\hat{\chi}'}(t) \tag{9}$$

The original aim of this cross-covariance maximisation is to account for the time lag between the time series w' and $\hat{\chi}'$ that is induced by sampling lines (air filters, tubing) and horizontal sensor separation, in other words to find such time lag that removes the $e^{-j\phi_{phys}}$ term in Eq. (2). After such successfully accounting for the travel time (t_{phys}), the attenuation of the measured cospectrum Co_m (and hence flux) would be described only by H, instead of H and H_p (see Eq. (4)), since the time lag estimation sets $H_p = 1$. However, the filter described by Eq. 3 results in a phase shift and hence produces an additional time lag between w' and $\hat{\chi}'$, i.e. t_{lpf}. This can be seen from Eq. (4): Q_m differs from zero when $\phi = 0$ (see also Massman (2000); Massman and Lee (2002); Wintjen et al. (2020)). Cross-covariance maximisation inadvertently derives the sum of t_{phys} and t_{lpf}, which implies that the time lag determined by cross-covariance maximisation is not the desired transport time lag. Using the sum of t_{phys} and t_{lpf} instead of t_{phys} induces a non-negligible negative ϕ in Eq. (4). Hence when shifting the time series according to the cross-covariance maximisation, the transfer function related to the phase shift (H_p) can no longer be neglected and should be calculated using $\phi = -\omega t_{lpf}$, where t_{lpf} is the bias in the time lag when estimated via cross-covariance maximisation, in other words the low-pass filtering induced time lag (note the minus-sign, since H_p accounts for the overestimated time lag).

As the maximal possible cospectral energy content per unit frequency can be described with the amplitude spectrum ($A_m = \sqrt{Co_m^2 + Q_m^2}$), it can be assumed that after the cross-covariance maximisation (time series shifted by $t_{phys} + t_{lpf}$), Co_m can be approximated by A_m. It is straightforward to derive A_m from Eq. (4):

$$A_m = \sqrt{Co_m^2 + Q_m^2} = \frac{Co}{\sqrt{1 + \omega^2 \tau^2}} = \sqrt{H} Co. \tag{10}$$

Hence A_m is attenuated with $\sqrt{H}$ instead of H which describes the attenuation of Co_m in the case that there is no phase shift between w' and $\hat{\chi}'$ as shown above. This suggests that after cross-covariance maximisation $\sqrt{H}$ approximates HH_p and the correct transfer function for cospectrum calculated after cross-covariance maximisation. However, $\sqrt{H}$ is not equivalent to HH_p This relates to the fact that Q_m cannot be nullified with a constant time shift since low-pass filtering induces a frequency-dependent time shift ($\frac{\arctan(-\omega \tau)}{\omega}$, see Massman (2000)). If Q_m could be nullified, then $Co_m = A_m$ (see Eq. (10)) and the attenuation of cospectra could be described accurately with $\sqrt{H}$. Note also that Eq. (10) applies universally, independent of ϕ.

The dependence between low-pass filtering induced time lag (t_{lpf}) and filter response time (τ) was estimated using the approximation $HH_p \approx \sqrt{H}$ or $H_p \approx \frac{1}{\sqrt{H}}$. For this analysis the phase transfer function H_p was approximated by using the series expansion of the terms in H_p (Eq. 6). This approximation resulted in $H_p \approx 1 - \frac{1}{2}(\omega t_{lpf})^2 + \omega\tau(\omega t_{lpf})$. Similarly, $\frac{1}{\sqrt{H}}$ can be approximated by $1 + \frac{1}{2}(\omega\tau)^2$. Equating these two approximations up to the second order yields a quadratic equation where the frequency dependence cancels out: $t_{lpf}^2 - 2\tau t_{lpf} + \tau^2 = 0$. The solution of this simple equation gives $t_{lpf} = \tau$. Thus, up to the second order approximation, which holds roughly up to the frequency value $\omega = 1$, the low pass filtering induced time lag equals the time constant of the filter. Note, however, that at this frequency range (ω between 0 and 1) the filtering effect is very weak. The dependence between t_{lpf} and τ can be determined also by numerically solving $H_p \approx \frac{1}{\sqrt{H}}$ (which equals $\cos(-2\pi f t_{lpf}) - \omega\tau\sin(-2\pi f t_{lpf}) \approx \sqrt{1 + (2\pi f \tau)^2}$) and using an assumption that t_{lpf} is proportional to τ, i.e. $t_{lpf} = C\tau$ where C is a proportionality constant. These analyses are continued in Sect. 4.1. Note that the dependency between t_{lpf} and τ derived here and in Sect. 4.1 was not used in the estimation of correction factors (see Sect. 3.2.1), but merely to analyse the factors controlling the dependency.

3 Materials and methods

3.1 Measurement sites

Measurements from the Siikaneva fen and the Hyytiälä forest site (SMEAR II) were used. Both stations are part of Integrated Carbon Observation System (ICOS) measurement station network.

The SMEAR II station is situated in Southern Finland ($61^o51'$ N, $24^o17'$ E; 181 m a.s.l.). The station is surrounded by extended areas of coniferous forests and the EC tower is located in a 57-year-old (in 2019) Scots pine (*Pinus sylvestris L.*) forest with a dominant tree height of ca. 19 m. The EC measurements were performed with 10 Hz sampling frequency at 27 m height, whereas the zero plane displacement height (d) was 14 m. The wind speed components and sonic temperature were measured by a 3-D ultrasonic anemometer (Solent Research HS1199, Gill Ltd, Lymington, UK), while carbon dioxide and water vapor mixing ratios were measured by an infrared gas analyzer (LI-7200, LI-COR Biosciences, Lincoln, NE, USA). A 0.77 m long tube (4 mm inner diameter) was used to sample air for the gas analyzer with a nominal flow rate of $10\,\mathrm{l\,min^{-1}}$. The centre of the sonic anemometer was displaced 20 cm horizontally and 1 cm vertically from the intake of the gas analyzer. The measurement setup was designed to closely follow the ICOS EC measurement protocols (Franz et al., 2018; Rebmann et al., 2018). The measurements were conducted between May and August 2019.

The Siikaneva fen site is located in Southern Finland ($61^o49.9610'$ N, $24^o11.5670'$ E; 160 m a.s.l), consisting mainly of sedges (*Eriophorum vaginatum, Carex rostrata, C. limosa*) and Sphagnum species, namely *S. balticum, S. majus* and *S. papillosum* with a height of ca. 10–30 cm. Further details about the site can be found in Riutta et al. (2007), Peltola et al. (2013) and Rinne et al. (2018). The EC measurements were conducted between May and August 2013. The data used in this study were measured with 10 Hz sampling frequency using a 3-D sonic anemometer (Metek USA- 1, GmbH, Elmshorn, Germany) and a closed-path analyzer (LI-7000, LI-COR Biosciences, Lincoln, NE, USA). The sonic anemometer and the gas

inlet were situated at 2.75 m above the peat surface, and the air was drawn to the analyzer through a 16.8 m long heated inlet sampling line. The center of the sonic anemometer was displaced 25 cm vertically above the intake of gas analyzer.

A short dataset (hereafter D_{S_1}) measured between 9:30 and 11:30 on 16-Jun 2013 at the Siikaneva site was used in the method validation (see Sect. 4.2), whilst long-term datasets from both Siikaneva (hereafter D_{S_2}) and Hyytiälä (hereafter D_H) were used to evaluate the accuracy of different spectral correction methods and their effect on CO_2 and H_2O fluxes (see Sect. 4.3).

3.2 Data processing

High frequency EC data from the two sites were processed in order to evaluate 1) the accuracy of different spectral correction methods and 2) their effect on gas (CO_2 and H_2O) flux estimates at these sites. The processing steps followed commonly accepted routines: 1) data were despiked using a method based on the running median filter (Brock, 1986; Starkenburg et al., 2016), 2) coordinates were rotated using double-rotation which aligned one of the horizontal wind components with the mean wind setting the mean vertical and cross wind components to zero, 3) gas (CO_2 and H_2O) mole fractions were converted point-by-point to be relative to dry air, if not already done internally by the gas analyser (LI-7200), 4) turbulent fluctuations were extracted from the measurements using block-averaging and 5) time lags between gas or filtered T (see Sect. 3.2.2) and vertical wind time series were accounted for using cross-covariance maximisation. Power spectra and cospectra were calculated after these processing steps. Spectral corrections and the related correction factors (CF) were calculated using four methods described below, see Sect. 3.2.1. After processing, the flux time series were quality filtered by removing periods with unrealistic sensible heat fluxes or friction velocities and highly non-stationary fluxes (Foken and Wichura, 1996). Site specific friction velocity thresholds (0.17 and 0.3 m/s for Siikaneva and Hyytiälä, respectively) were used to discard gas flux data during low turbulence periods. Furthermore, at Hyytiälä wind directions between $150°$ and $230°$ were discarded since here the mast construction disturbed the air flow. At Siikaneva an omnidirectional sonic anemometer was used mounted to the top of a mast and hence clearly disturbed wind directions were not identified. After quality filtering 4210 and 4722 30-min periods were available for analysis from Hyytiälä and Siikaneva, respectively.

Atmospheric stability was evaluated using the Obukhov length (L):

$$L = -\frac{u_*^3}{\frac{v_k g \overline{w'\theta_v'}}{\overline{\theta_v}}}, \tag{11}$$

where u_* is the friction velocity, $v_k = 0.4$ the von Karman constant, g the acceleration due to gravity and θ_v is virtual potential temperature. Overline denotes temporal averaging and primes deviations from the mean. From the Obukhov length, the stability parameter was calculated as $\zeta = \frac{z-d}{L}$, where z is the measurement height and d is the zero plane displacement height.

3.2.1 Empirical estimation of the low-pass filtering of the signal

The total transfer function of an EC setup can be estimated empirically from measured w-$\hat{\chi}$ and w-T cospectra:

$$H_{e,cs} = \frac{Co^{w,\hat{\chi}}}{Co^{w,T}} \frac{\overline{w'T'}}{\overline{w'\hat{\chi}'}} F_n, \tag{12}$$

or, alternatively, from the power spectra of the measured scalar and T:

$$H_{e,ps} = \frac{S_{\hat{\chi},\hat{\chi}}}{S_{T,T}} \frac{\sigma_T^2}{\sigma_{\hat{\chi}}^2} F_n, \tag{13}$$

where $Co^{w,\hat{\chi}}$ denotes the cospectral density between w and $\hat{\chi}$, and $\overline{w'\hat{\chi}'}$ represents the covariance between w and $\hat{\chi}$. $S_{\hat{\chi},\hat{\chi}}$ and $\sigma_{\hat{\chi}}^2$ denote the power spectral density and variance of $\hat{\chi}$, respectively, and the corresponding terms are defined for T. When

5 estimating $H_{e,cs}$ and $H_{e,ps}$, the covariances and variances were calculated from unattenuated frequencies (between 5×10^{-3} Hz and 5×10^{-2} Hz) (Foken et al., 2012a; Sabbatini et al., 2018). An additional normalisation factor (F_n) was also incorporated in order to take into account the fact that the variances and covariances in Eqs. (12) and (13) may be subject to various high frequency losses (Ibrom et al., 2007a). Here, w and T were approximated to be free from any low-pass filtering effects and thus $Co^{w,T}$ and $S_{T,T}$ could be used as a reference. $H_{e,cs}$ and $H_{e,ps}$ were calculated from ensemble-averaged spectra

10 from measurement periods that fulfilled the following criteria: flux stationarity (Foken and Wichura, 1996) was below 0.3, $u_* > 0.1 \mathrm{m\,s^{-1}}$, $\overline{w'T'} > 0.02 \mathrm{K\,m\,s^{-1}}$. For CO_2 it was also required that its turbulent flux was below -0.05 $\mu\mathrm{mol\,mol^{-1}\,m\,s^{-1}}$ and for H_2O it was required that the flux was directed upwards. For H_2O the transfer functions were determined in relative humidity (RH) bins and the τ and t_{lpf} values used in calculating CF were estimated from exponential fits made to the values obtained in the RH bins (similarly as for τ in Mammarella et al. (2009)). In the case of CO_2 and H_2O fluxes, the power spectra

15 were subjected to noise removal prior to utilising them in Eq. (13) by assuming that the signal was contaminated by white noise and that at the highest frequencies the power spectra contained only noise. See the influence of different noise removal techniques on the estimation of high frequency attenuation in our companion paper (Aslan et al., 2020).

Often both $H_{e,cs}$ and $H_{e,ps}$ are approximated by H with a value for τ that describes the low-pass filtering of the EC setup according to Eq. (5). Then the measured flux is corrected for low-pass filtering by multiplying it with CF (see Eq. (1)). There

20 are different ways to estimate $Co^{w,\chi}$ for Eq. (1). Here we limited the analysis only to periods when the absolute sensible heat fluxes were higher than 15 W m^{-2} and estimated $Co^{w,\chi}$ in Eq. (1) with the measured $Co^{w,T}$ following Fratini et al. (2012).

We used four methods to estimate EC system response times (and additionally t_{lpf} in Method 4) and then to calculate CF (see Table 1). All the four methods are subject to similar limitations, i.e. they are applicable only when the attenuation is not strong at frequencies close to the cospectral peak frequency. Method 1 follows the ICOS EC data processing protocol (Sabbatini

25 et al., 2018) and is implemented e.g. in EddyPro after Hunt et al. (2016) (see also https://www.licor.com/env/support/EddyPro/topics/whats-new.html). Method 2 follows Aubinet et al. (2000) and is implemented in EddyUH (Mammarella et al., 2016). Method 3 follows Fratini et al. (2012) and implemented in older versions of EddyPro, and Method 4 is the only one that explicitly accounts for the temporal lag caused by the low-pass filtering action of the system and is introduced in this study. In the Method 4, both parameters τ and t_{lpf}, were estimated by fitting HH_p to $H_{e,cs}$. Throughout the study, cross-covariance maximisation was used

30 to account for the lag between scalar and vertical wind speed as typically done in the global flux measurement network. Note that also other techniques have been used to estimate the time lag (e.g. Hunt et al., 2016; Taipale et al., 2010) and the selection of the time lag estimation method may have an effect on the correct shape of the cospectral transfer function (see Sect. 2). For instance, the cross-covariance moving average method to estimate the time lag introduced in Taipale et al. (2010) should be

Table 1. Methods used in this study to estimate flux losses and related correction factors (CF) due to low-pass filtering of the scalar signal. See the definitions for H and H_p in Eqs. (5) and (6), respectively. Values for τ (and t_{lpf} in Method 4) were estimated with non-linear least squares fit to $H_{e,ps}$ or $H_{e,cs}$ where F_n and τ (and t_{lpf} in Method 4) were used as fitting parameters. The additional normalisation factor F_n took into account any inaccuracies in estimation of variances and covariances in calculation of $H_{e,ps}$ or $H_{e,cs}$ (Eqs. (13) and (12)), respectively. The fits were weighted with temperature cospectra, in order to give more weight to frequencies where the scalar fluxes were high.

	Estimation of τ	Fitting parameters	H_{lpf} used in the estimation of CF, Eq. (1)	Reference
Method 1	fit H to $H_{e,ps}$	F_n, τ	H	Sabbatini et al. (2018)
Method 2	fit H to $H_{e,cs}$	F_n, τ	H	Aubinet et al. (2000)
Method 3	fit H to $H_{e,ps}$	F_n, τ	$\sqrt{H}$	Fratini et al. (2012)
Method 4	fit HH_p to $H_{e,cs}$	F_n, τ, t_{lpf}	HH_p	This study

related to Method 4 as it is also based on cross-covariance maximisation, whereas for the approach in Hunt et al. (2016) the correct cospectral transfer function is H (with the caveat that the physical time lag is estimated accurately).

3.2.2 Low-pass filtering of temperature data

In order to evaluate the performance of the different spectral correction methods presented in Sect. 3.2.1, high frequency T
5   time series were attenuated with different values of τ in order to mimic attenuated scalar time series. Similar to the procedure used by Aslan et al. (2020), T time series were converted to frequency domain via a Fourier transform, multiplied by Eq. (3) and converted back to time domain with the inverse Fourier transform. Three different values for τ were used: 0.1 s, 0.3 s and 0.7 s. The correct value for CF was obtained from the ratio between $\overline{w'T'}$ and $\overline{w'\hat{T}'}$, where $\hat{T}$ was the time series attenuated with the methodology described above. Note that here $\overline{w'\hat{T}'}$ was calculated using cross-covariance maximisation in order to
10   mimic regular EC gas flux processing, meaning that the lag caused by low-pass filtering was taken into account. This correct value for CF was then compared against CF estimated with the four methods described in Sect. 3.2.1 in order to evaluate the accuracy of the methods.

4   Results and discussion

4.1   Time lag dependence on attenuation and turbulence time scales

15   In Sect. 2.2, we explained why the following approximate relationship must hold up to some bound at the high frequency end: $H_p \approx 1/\sqrt{H}$. Using the assumption that $t_{lpf} = C\tau$, this equation was solved numerically for the constant C as a function of frequency f. Fig. 1 (upper plot) illustrates that such solution is dependent on frequency and varies over a relatively large interval up to the frequency $\frac{2}{3}\frac{\pi}{\tau}$ (the relationship holds well up to such frequency for any τ). This suggests that t_{lpf} and τ
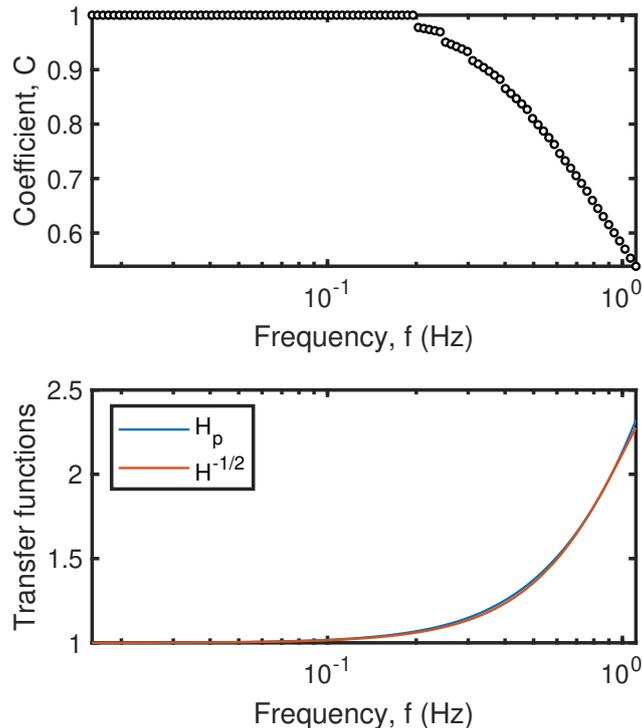
Figure 1. Top: the value for the proportionality constant C ($t_{lpf} = C\tau$) obtained when approximating $H_p \approx 1/\sqrt{H}$ at different frequency ranges. Bottom: H_p and $1/\sqrt{H}$ calculated using the proportionality $t_{lpf} = 0.63\tau$. See more details in Sect. 4.1.

are not directly proportional, but their relation depends on frequency. In accordance with the approximations with the Taylor expansion (Sect. 2.2), at low frequencies the constant C equals one. For illustration, the lower plot of Fig. 1 presents the left and right side terms of the approximate equality ($H_p \approx 1/\sqrt{H}$) calculated using a value 0.63 for the coefficient C. In spite of the large variation of the exact coefficient with frequency shown in the upper plot in Fig. 1, the selected constant value produces

5   very good correspondence for the whole frequency range suggesting that C can be approximated to be constant albeit strictly speaking it is not. The value of $C = 0.63$ was obtained by estimating the average time lag in a least square sense over equally spaced frequencies in logarithmic scale over the interval from $\tau = 0.01\frac{\pi}{\tau}$ to $\frac{2}{3}\frac{\pi}{\tau}$ for a range of time constants from 0.05 to 1 s. We observed that the optimum coefficient was independent of τ and equal to 0.63 (with 2-digit accuracy). Note that these analyses were independent of the actual turbulent signal as they were obtained using the transfer functions only (H and H_p).

10   In order to evaluate the influence of turbulent signal on the dependence between t_{lpf} and τ, the integral in Sect. 2.2, i.e. Eq. (9), was solved numerically with various combinations of time lag, τ and $(z-d)/U$ in order to evaluate which time lag value resulted in maximum value for the integral for a given τ and $(z-d)/U$ combination. This approach is similar to finding the time lag between signals using cross-covariance maximisation and it identified the dependence of the low-pass filtering induced lag (t_{lpf}) on τ and the turbulence time scale ($(z-d)/U$). For this numerical experiment, τ varied between 0.05 s and

15   1 s, $(z-d)/U$ between 1 s and 10 s and Co was calculated based on a model (similar to the one in Kristensen et al. (1997) but
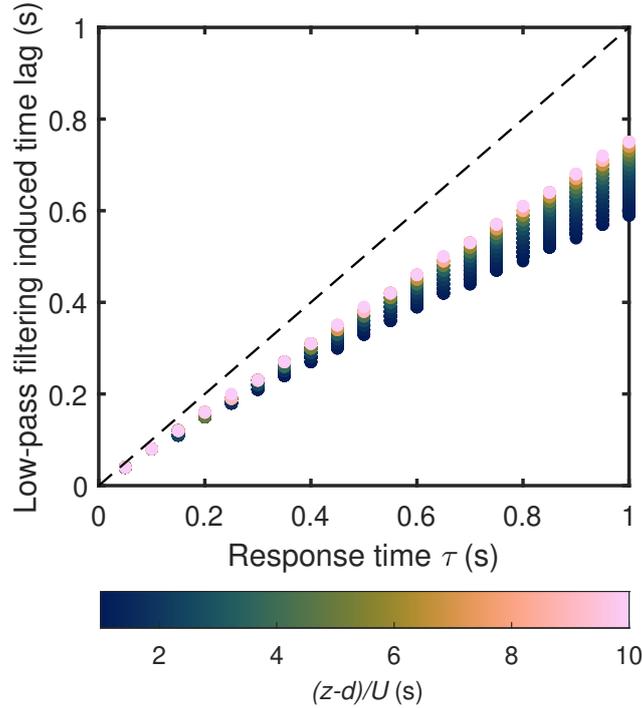
Figure 2. Low-pass filtering induced time lag (t_{lpf}) plotted against response time (τ). t_{lpf} values were estimated by numerically integrating the integral in Sect. 2.2 with various time lag values and evaluating which value resulted in maximum value for various τ and $(z-d)/U$ combinations. The dashed line shows 1:1 correspondence. See more details in Sect. 4.1.

fitted to Siikaneva observations). Based on this analysis, t_{lpf} depended approximately linearly on τ (Fig. 2) in accordance with the analysis above, yet the dependence had an additional weak $\frac{\tau U}{z-d}$ term: $t_{lpf} = a\tau - b\frac{\tau U}{z-d} + c$, where $a = 0.73$, $b = 0.15\,s$ and $c = 0.02\,s$. However, this numerical experiment was repeated also for very high attenuation levels and the found dependence above failed to fully recover t_{lpf} values at high attenuation and this bias increased with τ and inverse of turbulence time scale (i.e. $U/(z-d)$). For example at $\tau = 2\,s$ and $(z-d)/U = 1\,s$ the equation above gave $t_{lpf} = 1.2\,s$, whereas based on the numerical integration value 1.0 s was obtained, meaning that the dependence above was not able to accurately describe the low-pass induced time lag at these high attenuation levels. This is likely due to the fact that also the shape of the cospectrum Co in Eq. (9) has an effect on t_{lpf} dependence on τ. At very high attenuation levels also the peak of the cospectrum is attenuated and this results in a different t_{lpf} dependence on τ than the equation above which describes the dependence when attenuation takes place at high frequencies (i.e. inertial subrange).

The discrepancy between the two dependencies between t_{lpf} and τ obtained above was likely due to the fact that the latter took into account also the variability of the turbulent flux with frequency, whereas the former was based purely on transfer functions. Nevertheless, these results indicate that, for a given site, t_{lpf} can be approximated to be constant at a specific

11

attenuation (τ) level and hence supporting the estimation of t_{lpf} as a fitting parameter in the Method 4 when fitting HH_p to $H_{e,cs}$ (see Sect. 3.2.1 and Table 1).

4.2 Assessment of the flux loss correction methods using an attenuated T time series

The four methods to estimate the CF (Table 1) were evaluated using an artificially attenuated turbulent T time series comparing
5   different values for τ. Figure 3 shows example cross-covariance functions from the Siikaneva site with three different values
of τ applied to the same 2-hour time series. The peak of the w-$\hat{T}$ cross-covariance shifted to longer positive times (i.e. $\hat{T}$ lags
w) and the cross-covariance maximum decreased as τ increased. This is related to the phase shift and flux attenuation caused
by the low-pass filter, respectively. The low-pass filtering was also evident in the corresponding power spectra and cospectra.
The resulting empirical transfer functions in Fig. 4 show that power spectra were more attenuated than the cospectra, when
10   cospectra were calculated from data where the time lag derived from cross-covariance maximisation was used to shift the time
series (as is typically done when processing EC data). Moreover, the shape of the empirical transfer function derived from
the cospectra differed from Eq. (5). This difference in shape was related to H_p and the phase shift caused by the low-pass
filter. Note that the phase shift resulted in negative values for HH_p and $H_{e,cs}$ at high frequencies, meaning that the related
attenuated cospectrum had both positive and negative values. This implies that attenuated cospectra should not be presented
15   on log-log scales (negative values cannot be presented on log-scale). Note also that HH_p is not exactly equal to $\sqrt{H}$ at all
frequencies. In particular, HH_p shows negative values at high frequencies whereas $\sqrt{H}$ does not. Hence the approximation of
HH_p with $\sqrt{H}$ will likely fail under very strong attenuation. When the correction factor was calculated with Method 4, which
takes into account the low-pass filtering induced phase shift, the attenuation factors ($1/CF$) agree with the normalised cross-
covariance maxima (see Fig. 3). This indicates that the attenuation of cross-covariance maxima was accurately estimated with
20   this method. However, when H_p was neglected and the attenuation factors were calculated with H only, then they agreed with
cross-covariance values at zero lag as per predicted by theory (Sect. 2). Note that the time lag discussed here only represents
the low-pass filter effect, not other effects that also alter the time lag. This is only possible because we work with degraded
temperature time series, where phase shifts through low-pass filtering are the only cause for time delays.

    The value for τ used in attenuating the T time series was further varied between 0.05 s and 1 s and used for the same
25   2-hour time series. The bias in CF calculated with Method 1 increased with τ (Fig. 5a). The other methods did not produce
as significantly biased estimates for CF when using this example dataset, although Methods 2 and 3 somewhat underestimated
CF (approximately 4 % underestimation when τ=0.9 s) and this underestimation increased with τ. These findings are in
agreement with Fig. 4: $\sqrt{H}$ was above and H below the empirical transfer function calculated from the cospectrum ($H_{e,cs}$),
meaning that they underestimated and overestimated the attenuation, respectively. These findings are also in accordance with
30   Aslan et al. (2020) results with noisy measurements. Note that Method 2 estimated close to correct value for CF (Fig. 5a)
despite biased estimates for the response time (Fig. 5b) due to the compensation of two errors (biased τ and incorrect shape
for the cospectral transfer function). Method 4 was able to reproduce the correct value for τ from $H_{e,cs}$ (Fig. 5) indicating that
the difference between $H_{e,cs}$ and $H_{e,ps}$ was indeed related to H_p and the low-pass filtering related phase shift. The time lags
estimated by Method 4 (i.e. by fitting HH_p to $H_{e,cs}$) agreed with the ones estimated by maximising the crosscovariance (Fig.
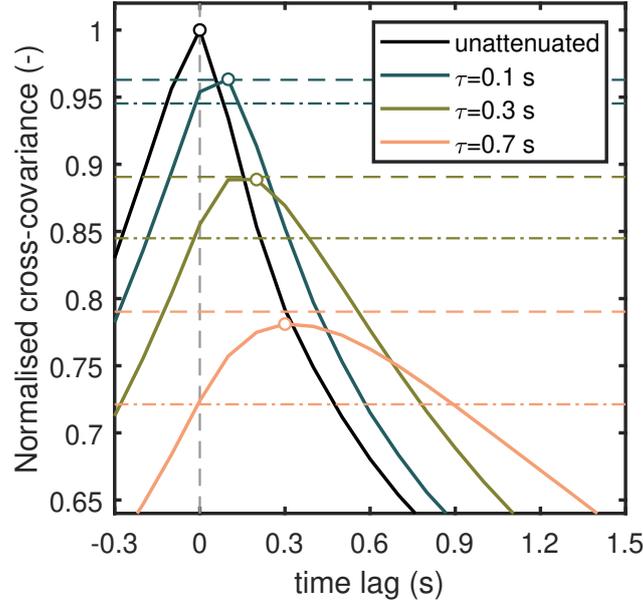
Figure 3. Cross-covariance between w and $\hat{T}$ calculated from data measured between 9:30 and 11:30 16.6.2013 at Siikaneva site. T data were attenuated with Eq. (3) and three different values for τ in order to demonstrate the effect of filtering on cross-covariance. All the cross-covariance values were normalised with maximum of unattenuated cross-covariance (i.e. unattenuated covariance). Dots highlight the maxima. Horizontal dashed lines show the attenuation factor (inverse of correction factor, $1/CF$) values calculated with Method 4 and dash-dot lines show the attenuation factors calculated with Method 1. Note that the dash-dot lines match the cross-covariance values at zero lag, whereas dashed lines agree with the cross-covariance maxima.
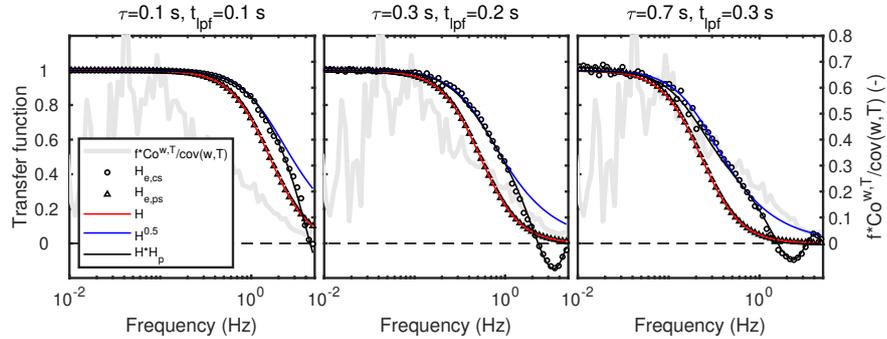
Figure 4. Transfer functions (left y-axes) and frequency-weighted and normalised cospectrum (right y-axes) for the same data shown in Fig. 3. Note that here H, $\sqrt{H}$ and HH_p were not fitted but calculated using the known values for τ and t_{lpf} resulting from the low-pass filtering of the T time series (Sect. 3.2.2). Nevertheless, H is related to Method 1, $H^{0.5}$ to Method 3 and HH_p to Method 4 (see Table 1). Note also that the cospectrum shown in the figure was calculated from the unattenuated T time series in order to demonstrate the frequency range having the biggest contribution to the flux.
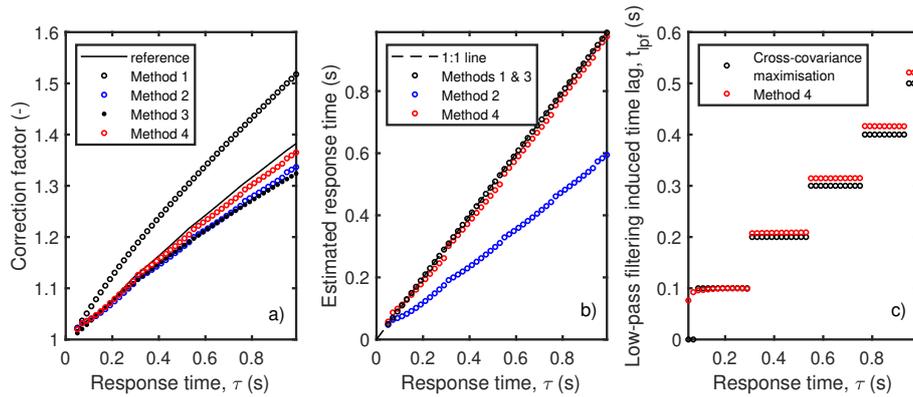
Figure 5. Comparison of estimated correction factors and response times to the values used to attenuate the T time series. The reference values for the correction factors were calculated as the ratio between $\overline{w'T'}$ and $\overline{w'\hat{T}'}$, where $\hat{T}$ is the temperature time series attenuated according to Sect. 3.2.2. Note that $\overline{w'\hat{T}'}$ was calculated using cross-covariance maximisation. The time lags obtained from cross-covariance maximisation and from fitting HH_p to $H_{e,cs}$ are shown in panel (c). The same data were used as in Figs. 3 and 4.

5c) also corroborating this conclusion. It should be noted that the step changes in the data that are very visible in Fig. 5c but to some extent also in Figs. 5a and b are caused by the finite resolution of the underlying data of w and T of 0.1 s.

In order to evaluate the four methods to estimate CF further, turbulent T data were low-pass filtered with three values of τ (0.1 s, 0.3 s and 0.7 s) over several summer months (May-August) at two contrasting EC sites, Hyytiälä and Siikaneva.

5　Then the related flux attenuation was corrected with the four methods and the results were compared against a reference flux calculated from unattenuated T data. Table 2 summarises the relative differences between the four correction methods and the reference. In general, the values obtained with this extended dataset are in line with Fig. 5a for Siikaneva albeit slight differences can be noted. The performance of all four methods decreases with increasing τ at both sites, and Method 1 showed the worst performance, which is in line with the example shown in Fig. 5 and follows the predictions from theory (Sect. 2). Of

10　the analysed cases, the biggest bias (+8.6 %) was found when applying Method 1 at Siikaneva with $\tau = 0.7\,s$. In general, the performance of the methods was worse at Siikaneva than at Hyytiälä. This was likely related to the lower measurement height at Siikaneva ($z-d$=2.7 m) than at Hyytiälä ($z-d$=13 m) and thus the comparably larger contribution of high frequencies to the covariance. At Siikaneva, smaller eddies dominated the turbulent transport and hence the effect of inaccuracies in describing the high frequency attenuation of the signal was amplified compared with Hyytiälä.

15　The importance of turbulence scale on the performance of the four methods was evaluated by stratifying the data according to stability and plotting them against τ/ITS (Fig. 6) where ITS is the integral time scale of $w'T'$, calculated from the auto-covariance of $w'T'$ time series by integrating the normalised autocovariance function until its first zero crossing (e.g. Kaimal and Finnigan, 1994). This ratio describes the ratio of attenuation and turbulent transport scales. It is also worth noting that this ratio can alternatively be approximated by the ratio of the cospectral peak frequency ($f_m = n_m U/(z-d)$, where n_m is the normalised cospectral peak frequency) to the cut-off frequency ($f_{co} = 1/(2\pi\tau)$) (Rannik et al., 2016). High values for τ/ITS

14

Table 2. Relative difference between the mean sensible heat fluxes obtained with the different correction methods ((cor-ref)/ref*100 %) and the reference (unattenuated sensible heat flux). All values are in %.

Site	Prescribed τ	Method 1	Method 2	Method 3	Method 4
Hyytiälä	0.1 s	+0.6	+0.2	+0.1	+0.3
Hyytiälä	0.3 s	+1.7	+0.6	+0.5	+0.7
Hyytiälä	0.7 s	+3.8	+1.0	+1.0	+1.5
Siikaneva	0.1 s	+2.4	-0.1	+0.2	-0.05
Siikaneva	0.3 s	+5.2	-0.5	-0.4	+0.3
Siikaneva	0.7 s	+8.6	-1.4	-1.5	+0.2

describe periods when the attenuation time scale is large relative to the time scale of turbulent scalar transport, whereas low values correspond to cases when the attenuation time scale is small relative to this turbulence scale. When CF was estimated with Methods 2 or 3, the relative bias in CF was typically within $\pm 3\%$ and increased linearly with τ/ITS at Siikaneva. The different behaviour of the two sites in Figs. 6b and 6c may be related to differences in spectral characteristics of turbulent

5   transport at these two sites since measurements in Hyytiälä were made above forest (roughness sublayer flow) and in Siikaneva above short vegetation (boundary layer flow). For Method 4 the bias was within $\pm 2\%$ at both sites and independent of the τ/ITS ratio. The remaining small bias obtained with Method 4 can be speculated to be related to the quadrature spectra, which was assumed to be zero, albeit strictly speaking it is not (Aslan et al., 2020). For Method 1 the relative bias in CF scaled with τ/ITS and after normalisation with ITS the data from both field sites collapsed into one common relationship (Fig. 6a). Horst

10 (1997) derived a simple formula to estimate CF for different situations as a function of $(\tau/\text{ITS})^\alpha$, where $\alpha = 7/8$ in neutral and unstable cases and $\alpha = 1$ in stable cases. Similar dependencies could be derived for the bias in CF derived with Method 1. However, these dependencies should not be used to rectify the biased CF values, rather CF should be estimated with methods that do not result in biased CF values in the first place.

Since the relative bias in CF when estimated with Method 1 scales with τ/ITS, this dependence can be used to assess

15 how much scalar fluxes are biased with different EC setups when the Method 1 is utilised in the EC data processing. For the following example calculations we approximate a linear dependence between ITS and $(z-d)/U$ and used the fit to estimate ITS for different $z-d$ and U combinations. For a short tower ($z-d$=1.5 m) with moderate wind speed ($U = 2$ m/s) and attenuation ($\tau = 0.2$ s), fluxes are biased by 4% based on the dependency shown in Fig. 6a. For the same tower, higher attenuation ($\tau = 0.8$ s) results in larger bias (9 %) if the Method 1 is utilised. For a tall tower the biases are not as significant since larger eddies

20 dominate the transport and hence τ/ITS is smaller for a given τ than in case of a shorter tower. For a tall tower ($z-d$=20 m), with moderate wind speed ($U = 3$ m/s) and attenuation ($\tau = 0.2$ s) the bias is 1-2% and with higher attenuation ($\tau = 0.8$ s) the bias is 3-4%. These example calculations demonstrate the magnitude of the flux bias resulting from biased spectral corrections at contrasting EC sites.
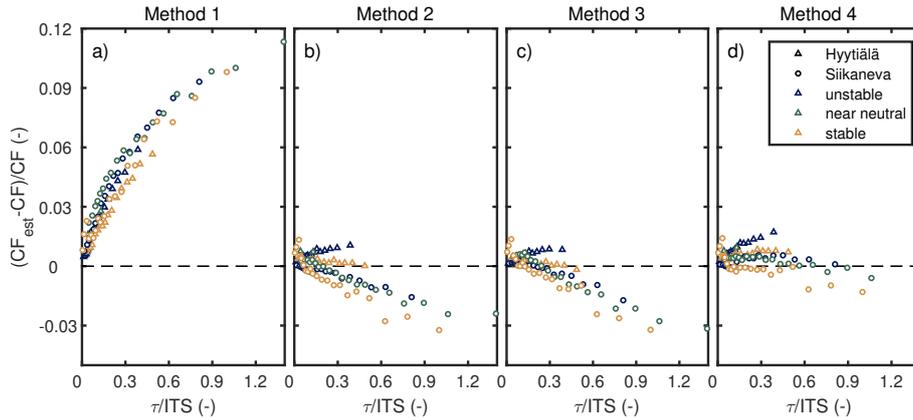
Figure 6. Relative bias in the estimated correction factor (CF_{est}) against τ/ITS where ITS is the integral time scale of $w'T'$. Data were divided into unstable ($\zeta < -0.1$), stable ($\zeta > 0.1$) and near-neutral ($|\zeta| < 0.1$) cases before bin-averaging and plotting. Reference values for the correction factor (CF in the figure) were calculated from the ratio between unattenuated and attenuated covariances. Note that the different colors refer to different stability conditions and markers to the different sites.

4.3 CO₂ and H₂O fluxes corrected with the four methods

The applicability of the results acquired with attenuated T was analysed by processing CO_2 and H_2O fluxes from summer months at the two sites (Sect. 3.1). The gas fluxes were corrected with the four spectral correction methods in order to assess the systematic biases stemming from biased spectral corrections. For CO_2 the fitting of H to $H_{e,ps}$, of H to $H_{e,cs}$ and of HH_p to

5   $H_{e,cs}$ estimated response times of 0.05 s, 0.10 s and 0.13 s at Hyytiälä and of 0.13 s, 0.12 s and 0.18 s at Siikaneva, respectively. The low-pass induced time lag (t_{lpf}) estimated as a fitting parameter when fitting HH_p to $H_{e,cs}$ yielded close to 0.1 s at both sites for CO_2. For reference, the time lags estimated via cross-covariance maximisation which are combinations of signal travel times in the sampling line (t_{phys}) and t_{lpf} yielded on average 1.4 s and 0.2 s at Siikaneva and Hyytiälä, respectively. For Hyytiälä the signal travel time calculated from the sampling tube dimensions and flow rate was 0.06 s. However, this calculation

10   neglects the additional time lag caused by LI-7550 Interface Unit and hence can be assumed to slightly underestimate t_{phys}.

Based on theoretical considerations (Sect. 2) and results obtained with attenuated T time series, H fit to $H_{e,cs}$ (Method 2) was projected to estimate smaller response time than the other two methods that were projected to agree (see e.g. Fig. 5b). Instead, here for CO_2 the HH_p fit to $H_{e,cs}$ gave longer response times than the other two methods (Fig. 7). For signals with small attenuation both τ and t_{lpf} are likely difficult to estimate accurately by fitting HH_p to $H_{e,cs}$. The low-pass filtering

15   induced lag (t_{lpf}) can attain values only with the temporal resolution of the data being processed (here 0.1 s) and hence for time series exhibiting small attenuation t_{lpf} may well be zero. This would cause $H_{e,ps}$ and $H_{e,cs}$ to be similar and hence they would result in similar estimates for the response time, as observed here for CO_2. This granular estimation of t_{lpf} might explain why the response times for CO_2 did not follow the expectations. It should be also noted that the methods to estimate the response time have a limited accuracy of estimation stemming from the algorithms used in the estimation, instrument limitations and
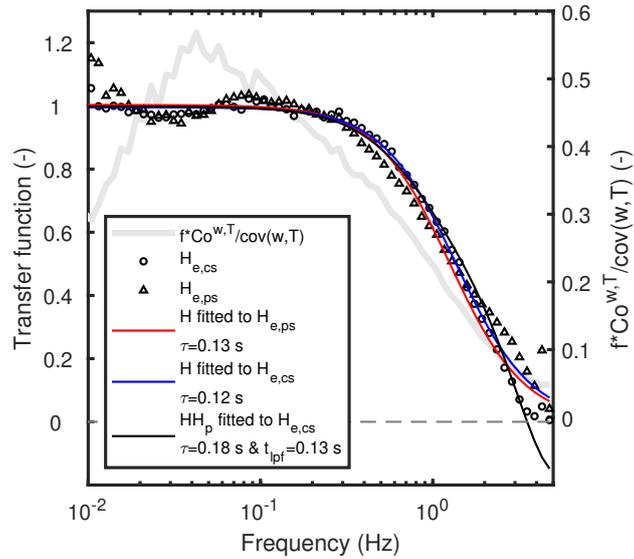
16

Figure 7. Empirical transfer functions estimated for CO_2 from ensemble averaged cospectra ($H_{e,cs}$, Eq. (12)) and power spectra ($H_{e,ps}$, Eq. (13)) and three fits to the empirical transfer functions. Also the corresponding frequency-weighted normalised average cospectrum related to heat flux is shown (grey line) in order to illustrate the frequency range with the highest contribution to the scalar fluxes. Data from Siikaneva were used.

meteorological conditions under which the observations are made (Aslan et al., 2020). Furthermore, the empirical transfer function derived from cospectra ($H_{e,cs}$) contains the attenuation related also to sensor separation (Horst and Lenschow, 2009), whereas the empirical transfer function estimated from power spectra ($H_{e,ps}$) is related only to gas analyser induced low-pass filtering.

5   For H_2O, τ depends on RH (Mammarella et al., 2009; Ibrom et al., 2007a; Runkle et al., 2012) and hence the analysis was done in RH bins. Figure 8 shows an example of empirically derived transfer functions for H_2O at Siikaneva in moderate relative humidity conditions. $H_{e,cs}$ showed less high frequency attenuation than $H_{e,ps}$ due to cross-covariance maximisation as predicted by the theory (Sect. 2). HH_p fit to $H_{e,cs}$ resulted in similar value for τ as the one obtained by fitting H to $H_{e,ps}$. The other fitting parameter in HH_p fit (t_{lpf}) was 0.14 s indicating the low-pass filtering of H_2O time series caused an additional lag
10   to the H_2O time series. Note that H does not perfectly describe the shape of $H_{e,ps}$. This is due to adsorption and desorption of H_2O to sampling tube walls, a process which cannot be described accurately with Eq. (3) (Nordbo et al., 2013). Hence different transfer functions have been proposed for H_2O (De Ligne et al., 2010; Nordbo et al., 2014).

Figure 9 shows results obtained for H_2O in different RH bins at the two sites. The H fit to $H_{e,cs}$ (Method 2) gave smaller values for τ in agreement with the results obtained with attenuated T (Fig. 5b) and expectations based on the theory (Sect. 2).
15   The HH_p fit to $H_{e,cs}$ (Method 4) was able to reproduce the H_2O time lag dependency on RH, yet it estimated systematically smaller values for the time lag difference between H_2O and CO_2 than obtained with cross-covariance maximisation. The time lag difference between H_2O and CO_2 can be assumed to be related to t_{lpf} of H_2O since H_2O is more attenuated than CO_2.
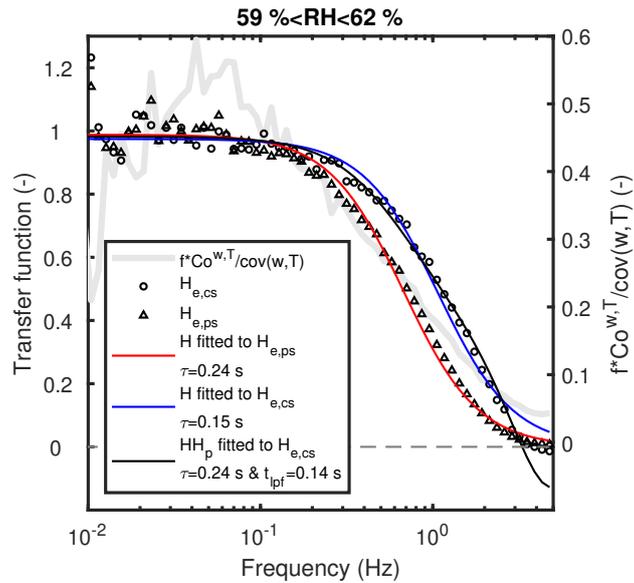
Figure 8. Similar figure as Fig. 7 but for H_2O in moderate relative humidity conditions (59%<RH<62%). Note that τ estimated from $H_{e,ps}$ agrees with τ estimated from $H_{e,cs}$ with HH_p. Data from Siikaneva were used.

The difference between H_2O and CO_2 time lags obtained with cross-covariance maximisation showed linear dependence on estimated response times in relative humidity bins with a similar dependency at both sites ($y = ax + b$, where $a = 0.47$ and $b = -0.05\,s$ for Siikaneva and $a = 0.44$ and $b = -0.07\,s$ for Hyytiälä, where y is the time lag difference and x response time. Fits were based on orthogonal linear regression). Difference between H_2O and CO_2 time lags resulted from stronger low-pass

5   filtering of H_2O than CO_2 signal and this analysis assumes that the mere travel times through the sampling lines (i.e. t_{phys}), which do not depend on the low-pass filtering effects, were the same for H_2O and CO_2. These results are in line with Fig. 2 where it was shown that the low-pass filtering induced time lag was primarily determined by a linear dependence on τ with a secondary dependence on turbulence time scale. However, the slopes obtained above were different from the ones derived in Sect. 4.1.

10   The CF values estimated with the four methods agreed at Hyytiälä for low RH periods, but they diverged at high RH periods. For instance when RH>80 % the four methods gave on average 1.39, 1.29, 1.23 and 1.37 at the Hyytiälä site, respectively. These results are in line with the ones obtained with attenuated T time series (Sect. 4.2 and Fig. 5a): when τ was large, Method 1 overestimated and Method 3 underestimated CF similarly as here for H_2O at high RH (and hence large τ). In contrast, for Siikaneva Method 1 gave systematically higher value for the correction factor regardless of RH, whereas the other three

15   methods gave more similar CF RH dependency. This difference to Hyytiälä was likely due to lower τ values also at high RH (Fig. 9). Note also that the EC measurement setup (measurement height, gas sampling system) was not identical at the two sites.
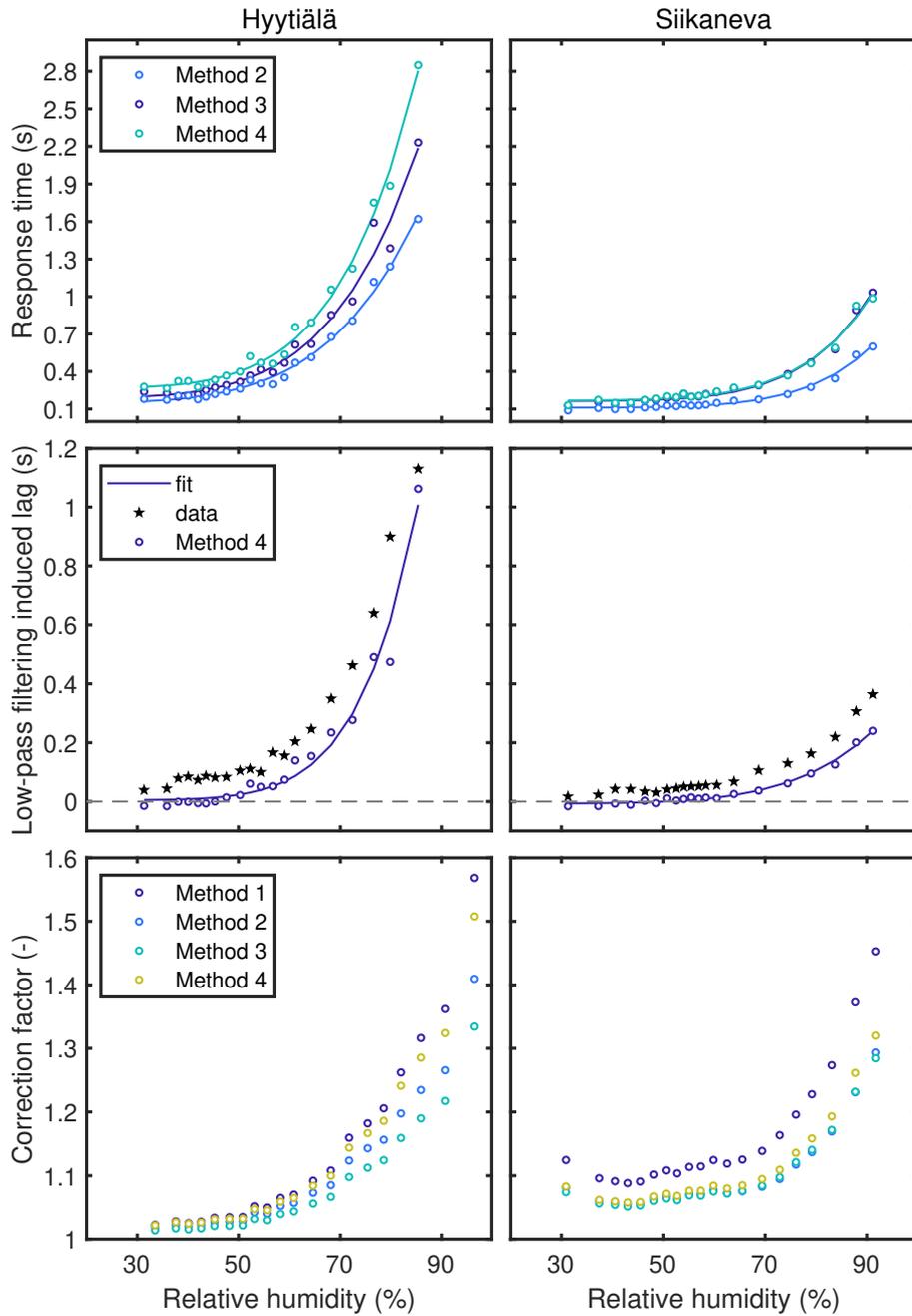
Figure 9. Response times (top row), low-pass filtering induced time lags (middle row) and correction factors (bottom row) as a function of relative humidity. Results for Hyytiälä pine forest are on the left and for Siikaneva open peatland on the right. The lines describe the fits used to obtain τ and t_{lpf} values for the CF calculation (see Sect. 3.2.1).

Table 3. Relative difference between the mean CO_2 and H_2O fluxes obtained with the different correction methods ((cor-ref)/ref*100 %). Fluxes corrected with Method 4 were used as a reference for the other three methods. All values are in %.

Site	Gas flux	Method 1			Method 2			Method 3		
		All	Night	Day	All	Night	Day	All	Night	Day
Hyytiälä	CO_2	-0.5	-0.7	-0.5	+0.07	+0.1	+0.08	-0.7	-1.0	-0.7
Hyytiälä	H_2O	+0.7	+1.6	+0.7	-1.0	-1.4	-1.0	-2.3	-4.0	-2.3
Siikaneva	CO_2	+0.4	+0.3	+0.4	-0.3	-0.2	-0.3	-2.4	-1.9	-2.4
Siikaneva	H_2O	+4.1	+4.7	+4.1	-0.6	-0.8	-0.6	-1.0	-1.0	-1.0

On average, the differences between the four different methods to calculate CF were small, typically within $\pm 3\%$ at both sites for both gases (CO_2 and H_2O) (Table 3). The biggest mean relative difference (4.1%) was found for H_2O measurements at Siikaneva site for Method 1. This was likely due to the combination of low measurement height and high attenuation which resulted in biased CF values, in accordance with the findings obtained with the attenuated T time series (Fig. 6a). Interestingly, for CO_2 the biggest difference at both sites was obtained with Method 3, yielding smaller fluxes than the reference (Method 4). The difference was bigger than the one obtained with Method 1 which contradicts the findings presented above with attenuated T (Sect. 4.2 and Table 2) and expectations based on theory (Sect. 2), albeit the found differences between the Methods were generally small. Note that if $t_{lpf} \approx 0$, then both power spectra and cospectra are attenuated similarly (i.e. with H) yielding Methods 1, 2 and 4 to be similar. Infrared gas analysers for CO_2 and H_2O can often be mounted close to the inlet and in both setups considered here inlet lines are fairly short. The measurement of other gases, incl. CH_4 and N_2O, usually require larger equipment which often has to operated on the ground and/or some distance away from the mast, requiring longer inlet lines with slow time-response. In these situations the correct shape of the cospectral transfer function matters a lot more than for the measurement setups included here and hence the variability between methods is expected to be larger.

4.4 Correct form for cospectral transfer function

There has been a long-standing debate about what is the correct form for cospectral transfer function when the scalar measurements are done with first-order linear sensor and vertical wind speed is not attenuated. The seminal paper on EC frequency-response corrections by Moore (1986) described the flux attenuation related to the scalar sensor with $\sqrt{H}$ (see Eq. (5)), which was later deemed erroneous, e.g. by Eugster and Senn (1995); Horst (1997, 2000) and others. Partly based on similar derivations as shown here in Sect. 2, the correct form for the cospectral transfer function was argued by Horst (1997, 2000) and Massman (2000) to be H, instead of $\sqrt{H}$. Lately, both forms (H and $\sqrt{H}$) have been utilised in the literature (e.g. Fratini et al., 2012; Foken et al., 2012b; Mammarella et al., 2016; Hunt et al., 2016; Wintjen et al., 2020) without clear consensus on which one is correct. Part of this confusion is likely related to the fact that some of the past studies have been using incorrect

terminology by using the term cospectral transfer function (Eq. (5)), even though they have derived/utilised transfer function for the amplitude spectrum (Eq. (10)).

Briefly summarising the findings in this study, it was shown in Sect. 2 in accordance with e.g. Horst (2000) that in the case the travel time in the gas sampling system could be accurately estimated and accounted for, the attenuation of cospectrum (and hence flux) could be described with H. However, cross-covariance maximisation inadvertently accounts also for the scalar low-pass filtering related time shift (t_{lpf}) and consequently induces a phase shift between the lag corrected attenuated scalar and vertical wind time series. Hence in the case that cross-covariance maximisation is used to align the two time series, the correct form for cospectral transfer function is HH_p, where the part related to the phase shift (H_p) is calculated with t_{lpf}. It was shown above that HH_p can be approximated with $\sqrt{H}$. Therefore the debate about which is the correct form for cospectral transfer function (H or $\sqrt{H}$) relates to the low-pass filtering induced phase shift as discussed already by Eugster and Senn (1995) and Horst (2000), albeit with a different conclusion. Note however, that $\sqrt{H}$ is an approximation, not an exact representation of the cospectral transfer function.

5   Summary and conclusions

The influence of low-pass filtering induced phase shift on estimation of high frequency response of an EC setup was analysed. The analysis assumed that the EC setup consisted of a fast-response anemometer and a linear, first-order-response scalar sensor. Spectral corrections aiming at correcting the EC fluxes for low-pass filtering were estimated with four methods: three widely used methods and one newly proposed method which specifically accounts for the interaction between the low-pass filtering induced phase shift and attenuation. Based on theoretical considerations and experimental results we come to the following conclusions:

– Cross-covariance maximisation overestimates the signal travel time in the EC sampling line since it inadvertently accounts also for the lag caused by low-pass filtering of scalar time series caused by non-ideal measurement system. The bias in the estimated time lag depends linearly on low-pass filter response time (τ) with a small additional dependence on turbulence time scale. Hence, other means for estimating the physical time lag might be warranted, especially in the case of noisy measurements (Langford et al., 2015). Further research on this topic is required.

– Both power spectra and cospectra are attenuated with the same transfer function (H, as noted also by Horst (2000)) in the case that the travel time of the scalar signal in the sampling line can be accurately estimated. However, if cross-covariance maximisation is used, then attenuation of cospectra follows HH_p where H_p accounts for the bias in the estimated travel time caused by cross-covariance maximisation and it was shown that HH_p can be roughly approximated with $\sqrt{H}$. Therefore, all flux calculation algorithms which rely on cross-covariance maximisation and at the same time use H to describe the attenuation of the cospectra (e.g. Horst, 1997; Massman, 2000) can be projected to be biased in the same way as Method 1 used here if the response time (i.e. τ) is accurately estimated (e.g. from power spectra). In these cases the bias in EC fluxes can be 10% or above for short tower measurements with moderate attenuation. Hence, data reprocessing is warranted in order to rectify this bias.

- In order to estimate and correct for the flux attenuation correctly, it is vital to accurately describe the attenuation of the cospectra in the correction procedure. Hence, while fitting H to cospectra (Method 2) biased the first-order response time due to the use of the incorrect cospectral transfer function, it resulted only in a small bias for the flux correction factor, since the method describes the attenuation of cospectra accurately once the cross-covariance maximisation has been applied. By contrast, fitting of H to power-spectra (Method 1) correctly estimates the response time, but it nevertheless yields biased flux corrections since it utilised a transfer function that is incorrect when estimating the flux using cross-covariance maximisation.

- The theoretical framework proposed in this paper was able to describe the changes in H_2O time lag as H_2O response time increased with relative humidity. This suggests that the findings derived here with attenuated temperature time series are applicable also in real world situations for EC gas flux measurements. However, results for CO_2 deviated from the expectations made based on the theory. Reasons for this remained unclear, however low-pass filtering of inert gases (such as CO_2) in the gas sampling line may deviate from what was described here in such a way that the low-pass filter acting on CO_2 may not induce a phase shift. This should be investigated by using CO_2 flux data from an EC setup with pronounced attenuation of CO_2 fluctuations in the sampling line or alternatively in a controlled environment in a laboratory (Metzger et al., 2016; Aubinet et al., 2016).

In summary, it is suggested that the spectral correction methods implemented in EC data processing software are revised so that the influence of low-pass filtering induced phase shift is recognised following the findings presented above. In particular, the usage of Method 1 is discouraged as it resulted in clearly biased flux values.

Code and data availability. Data and matlab codes to reproduce Figures 3, 4 and 5 will be uploaded to open data repository Zenodo upon acceptance of this manuscript along with flux time series processed with the four methods (Table 1) at the two sites.

Appendix A: Derivation of Eq. (4)

Here we derive Eq. (4) starting from the cross-spectrum (Eq. (2)):

$$Cr_m = [Z_w] [h_\chi Z_\chi]^* e^{-j\phi_{phys}}, \tag{A1}$$

where h_χ can be described with Eq. (3), which gives

$$Cr_m = [Z_w] \left[\frac{Z_\chi}{1 - j\omega\tau} \right]^* e^{-j\phi_{phys}} \tag{A2}$$

$$Cr_m = [Z_w] \left[\frac{Z_\chi^*}{1 + j\omega\tau} \right] e^{-j\phi_{phys}} \tag{A3}$$

$$Cr_m = Z_w Z_\chi^* \frac{1}{1 + j\omega\tau} e^{-j\phi_{phys}} \tag{A4}$$

$$Cr_m = \frac{Co + jQ}{1 + j\omega\tau} e^{-j\phi_{phys}} \tag{A5}$$

$$Cr_m = \frac{(Co + jQ)(1 - j\omega\tau)}{1 + \omega^2\tau^2} e^{-j\phi_{phys}} \tag{A6}$$

$$Cr_m = \frac{(Co - j\omega\tau Co + jQ + \omega\tau Q)}{1 + \omega^2\tau^2} e^{-j\phi_{phys}}, \tag{A7}$$

where $Z_w Z_\chi^* = Co + jQ$ was utilised. Next quadrature spectrum (Q) was assumed zero (Horst, 1997; Massman, 2000) and hence

$$Cr_m = \frac{Co - j\omega\tau Co}{1 + \omega^2\tau^2} e^{-j\phi_{phys}} \tag{A8}$$

Now we can use Euler formula ($e^{-j\phi_{phys}} = \cos\phi_{phys} - j\sin\phi_{phys}$)

$$Cr_m = \frac{Co - j\omega\tau Co}{1 + \omega^2\tau^2} (\cos\phi_{phys} - j\sin\phi_{phys}) \tag{A9}$$

$$Cr_m = \frac{Co\cos\phi_{phys} - j\omega\tau Co\cos\phi_{phys} - jCo\sin\phi_{phys} - \omega\tau Co\sin\phi_{phys}}{1 + \omega^2\tau^2} \tag{A10}$$

$$Cr_m = \frac{\cos\phi_{phys} - \omega\tau\sin\phi_{phys}}{1 + \omega^2\tau^2} Co - j\frac{\sin\phi_{phys} + \omega\tau\cos\phi_{phys}}{1 + \omega^2\tau^2} Co \tag{A11}$$

which equals the Eq. (4) in Sect. 2.

References

Aslan, T., Peltola, O., Ibrom, A., Nemitz, E., Rannik, , and Mammarella, I.: The high frequency response correction of eddy covariance fluxes.Part 1: an experimental approach for analysing noisy measurements of small fluxes, Atmospheric Measurement Techniques Discussions, submitted, 2020.

5 Aubinet, M., Grelle, A., Ibrom, A., Rannik, U., Moncrieff, J., Foken, T., Kowalski, A. S., Martin, P. H., Berbigier, P., Bernhofer, C., Clement, R., Elbers, J., Granier, A., Grunwald, T., Morgenstern, K., Pilegaard, K., Rebmann, C., Snijders, W., Valentini, R., and Vesala, T.: Estimates of the annual net carbon and water exchange of forests: The EUROFLUX methodology, ADVANCES IN ECOLOGICAL RESEARCH, 30, 113–175, 2000.

Aubinet, M., Vesala, T., and Papale, D.: Eddy covariance : a practical guide to measurement and data analysis, Springer Atmospheric Sciences., Springer, Dordrecht :, http://helka.linneanet.fi/cgi-bin/Pwebrecon.cgi?BBID=2391473, 2012.

Aubinet, M., Joly, L., Loustau, D., De Ligne, A., Chopin, H., Cousin, J., Chauvin, N., Decarpenterie, T., and Gross, P.: Dimensioning IRGA gas sampling systems: laboratory and field experiments, Atmos. Meas. Tech., 9, 1361–1367, https://doi.org/10.5194/amt-9-1361-2016, https://www.atmos-meas-tech.net/9/1361/2016/https://www.atmos-meas-tech.net/9/1361/2016/amt-9-1361-2016.pdf, 2016.

Baldocchi, D. D.: Assessing the eddy covariance technique for evaluating carbon dioxide exchange rates of ecosystems: past, present and future, Global Change Biology, 9, 479–492, https://doi.org/10.1046/j.1365-2486.2003.00629.x, 2003.

15 Brock, F. V.: A Nonlinear Filter to Remove Impulse Noise from Meteorological Data, Journal of Atmospheric and Oceanic Technology, 3, 51–58, https://doi.org/10.1175/1520-0426(1986)003<0051:ANFTRI>2.0.CO;2, http://dx.doi.org/10.1175/1520-0426(1986)003%3C0051: ANFTRI%3E2.0.CO;2http://journals.ametsoc.org/doi/pdf/10.1175/1520-0426%281986%29003%3C0051%3AANFTRI%3E2.0.CO% 3B2, 1986.

20 De Ligne, A., Heinesch, B., and Aubinet, M.: New Transfer Functions for Correcting Turbulent Water Vapour Fluxes, Boundary-Layer Meteorology, 137, 205–221, https://doi.org/10.1007/s10546-010-9525-9, https://doi.org/10.1007/s10546-010-9525-9, 2010.

Eugster, W. and Senn, W.: A Cospectral Correction Model for Measurement of Turbulent No2 Flux, Boundary-Layer Meteorology, 74, 321–340, https://doi.org/10.1007/BF00712375, 1995.

Foken, T. and Wichura, B.: Tools for quality assessment of surface-based flux measurements, Agricultural and Forest Meteorology, 78, 25 83–105, 1996.

Foken, T., Aubinet, M., and Leuning, R.: The Eddy Covariance Method, in: Eddy Covariance, edited by Aubinet, M., Vesala, T., and Papale, D., Springer Atmospheric Sciences, chap. 1, pp. 1–19, Springer Netherlands, https://doi.org/10.1007/978-94-007-2351-1_1, http://dx.doi.org/10.1007/978-94-007-2351-1_1, 2012a.

Foken, T., Leuning, R., Oncley, S. R., Mauder, M., and Aubinet, M.: Corrections and Data Quality Control BT - Eddy Covariance: A Practical 30 Guide to Measurement and Data Analysis, pp. 85–131, Springer Netherlands, Dordrecht, https://doi.org/10.1007/978-94-007-2351-1_4, https://doi.org/10.1007/978-94-007-2351-1_4, 2012b.

Franz, D., Acosta, M., Altimir, N., Arriga, N., Arrouays, D., Aubinet, M., Aurela, M., Ayres, E., López-Ballesteros, A., Barbaste, M., Berveiller, D., Biraud, S., Boukir, H., Brown, T., Brömmer, C., Buchmann, N., Burba, G., Carrara, A., Cescatti, A., Ceschia, E., Clement, R., Cremonese, E., Crill, P., Darenova, E., Dengel, S., D'Odorico, P., Filippa, G., Fleck, S., Fratini, G., Fuß, R., Gielen, B., Gogo, S., 35 Grace, J., Graf, A., Grelle, A., Gross, P., Grönwald, T., Haapanala, S., Hehn, M., Heinesch, B., Heiskanen, J., Herbst, M., Herschlein, C., Hörtnagl, L., Hufkens, K., Ibrom, A., Jolivet, C., Joly, L., Jones, M., Kiese, R., Klemedtsson, L., Kljun, N., Klumpp, K., Kolari, P., Kolle, O., Kowalski, A., Kutsch, W., Laurila, T., De Ligne, A., Linder, S., Lindroth, A., Lohila, A., Longdoz, B., Mammarella, I., Manise,

T., Jiménez, S., Matteucci, G., Mauder, M., Meier, P., Merbold, L., Mereu, S., Metzger, S., Migliavacca, M., Mölder, M., Montagnani, L., Moureaux, C., Nelson, D., Nemitz, E., Nicolini, G., Nilsson, M., De Beeck, M., Osborne, B., Löfvenius, M., Pavelka, M., Peichl, M., Peltola, O., Pihlatie, M., Pitacco, A., Pokorný, R., Pumpanen, J., Ratié, C., Rebmann, C., Roland, M., Sabbatini, S., Saby, N., Saunders, M., Schmid, H., Schrumpf, M., Sedlák, P., Ortiz, P., Siebicke, L., Šigut, L., Silvennoinen, H., Simioni, G., Skiba, U., Sonnentag, O., Soudani, K., Soulé, P., Steinbrecher, R., Tallec, T., Thimonier, A., Tuittila, E.-S., Tuovinen, J.-P., Vestin, P., Vincent, G., Vincke, C., Vitale, D., Waldner, P., Weslien, P., Wingate, L., Wohlfahrt, G., Zahniser, M., and Vesala, T.: Towards long-Term standardised carbon and greenhouse gas observations for monitoring Europe's terrestrial ecosystems: A review, International Agrophysics, 32, https://doi.org/10.1515/intag-2017-0039, 2018.

Fratini, G., Ibrom, A., Arriga, N., Burba, G., and Papale, D.: Relative humidity effects on water vapour fluxes measured with closed-path eddy-covariance systems with short sampling lines, Agricultural and Forest Meteorology, 165, 53–63, https://doi.org/http://dx.doi.org/10.1016/j.agrformet.2012.05.018, http://www.sciencedirect.com/science/article/pii/S0168192312001955, 2012.

Horst, T. W.: A simple formula for attenuation of eddy fluxes measured with first-order-response scalar sensors, Boundary-Layer Meteorology, 82, 219–233, 1997.

Horst, T. W.: On Frequency Response Corrections for Eddy Covariance Flux Measurements, Boundary-Layer Meteorology, 94, 517–520, https://doi.org/10.1023/A:1002427517744, https://doi.org/10.1023/A:1002427517744, 2000.

Horst, T. W. and Lenschow, D. H.: Attenuation of Scalar Fluxes Measured with Spatially-displaced Sensors, Boundary-Layer Meteorology, 130, 275–300, https://doi.org/10.1007/s10546-008-9348-0, http://dx.doi.org/10.1007/s10546-008-9348-0, 2009.

Hunt, J. E., Laubach, J., Barthel, M., Fraser, A., and Phillips, R. L.: Carbon budgets for an irrigated intensively grazed dairy pasture and an unirrigated winter-grazed pasture, Biogeosciences, 13, 2927–2944, https://doi.org/10.5194/bg-13-2927-2016, https://bg.copernicus.org/articles/13/2927/2016/https://bg.copernicus.org/articles/13/2927/2016/bg-13-2927-2016.pdf, 2016.

Ibrom, A., Dellwik, E., Flyvbjerg, H., Jensen, N. O., and Pilegaard, K.: Strong low-pass filtering effects on water vapour flux measurements with closed-path eddy correlation systems, Agricultural and Forest Meteorology, 147, 140–156, https://doi.org/10.1016/j.agrformet.2007.07.007, 2007a.

Ibrom, A., Dellwik, E., Larsen, S. E., and Pilegaard, K.: On the use of the Webb-Pearman-Leuning theory for closed-path eddy correlation measurements, Tellus Series B-Chemical and Physical Meteorology, 59, 937–946, https://doi.org/10.1111/j.1600-0889.2007.00311.x, 2007b.

Kaimal, J. C. and Finnigan, J. J.: Atmospheric boundary layer flows : their structure and measurement, Oxford University Press, New York, http://helka.linneanet.fi/cgi-bin/Pwebrecon.cgi?BBID=636956, 1994.

Kristensen, L., Mann, J., Oncley, S. P., and Wyngaard, J. C.: How Close is Close Enough When Measuring Scalar Fluxes with Displaced Sensors?, Journal of Atmospheric and Oceanic Technology, 14, 814–821, https://doi.org/10.1175/1520-0426(1997)014<0814:HCICEW>2.0.CO;2, https://doi.org/10.1175/1520-0426(1997)014%3C0814:HCICEW%3E2.0.COhttp://0.0.0.2, 1997.

Langford, B., Acton, W., Ammann, C., Valach, A., and Nemitz, E.: Eddy-covariance data with low signal-to-noise ratio: time-lag determination, uncertainties and limit of detection, Atmos. Meas. Tech., 8, 4197–4213, https://doi.org/10.5194/amt-8-4197-2015, http://www.atmos-meas-tech.net/8/4197/2015/http://www.atmos-meas-tech.net/8/4197/2015/amt-8-4197-2015.pdf, 2015.

Mammarella, I., Launiainen, S., Gronholm, T., Keronen, P., Pumpanen, J., Rannik, U., and Vesala, T.: Relative Humidity Effect on the High-Frequency Attenuation of Water Vapor Flux Measured by a Closed-Path Eddy Covariance System, Journal of Atmospheric and Oceanic Technology, 26, 1856–1866, https://doi.org/10.1175/2009JTECHA1179.1, 2009.

Mammarella, I., Nordbo, A., Rannik, U., Haapanala, S., Levula, J., Laakso, H., Ojala, A., Peltola, O., Heiskanen, J., Pumpanen, J., and Vesala, T.: Carbon dioxide and energy fluxes over a small boreal lake in Southern Finland, Journal of Geophysical Research : Biogeosciences, 120, 1296–1314, https://doi.org/10.1002/2014JG002873, 2015.

Mammarella, I., Peltola, O., Nordbo, A., Järvi, L., and Rannik, : Quantifying the uncertainty of eddy covariance fluxes due to the use of different software packages and combinations of processing steps in two contrasting ecosystems, Atmospheric Measurement Techniques, 9, 4915–4933, https://doi.org/10.5194/amt-9-4915-2016, 2016.

Massman, W. J.: A simple method for estimating frequency response corrections for eddy covariance systems, Agricultural and Forest Meteorology, 104, 185–198, https://doi.org/10.1016/S0168-1923(00)00164-7, 2000.

Massman, W. J. and Lee, X.: Eddy covariance flux corrections and uncertainties in long-term studies of carbon and energy exchanges, Agricultural and Forest Meteorology, 113, 121–144, 2002.

Metzger, S., Burba, G., Burns, S. P., Blanken, P. D., Li, J., Luo, H., and Zulueta, R. C.: Optimization of an enclosed gas analyzer sampling system for measuring eddy covariance fluxes of H2O and CO2, Atmos. Meas. Tech., 9, 1341–1359, https://doi.org/10.5194/amt-9-1341-2016, https://www.atmos-meas-tech.net/9/1341/2016/https://www.atmos-meas-tech.net/9/1341/2016/amt-9-1341-2016.pdf, 2016.

Moncrieff, J. B., Massheder, J. M., deBruin, H., Elbers, J., Friborg, T., Heusinkveld, B., Kabat, P., Scott, S., Soegaard, H., and Verhoef, A.: A system to measure surface fluxes of momentum, sensible heat, water vapour and carbon dioxide, Journal of Hydrology, 189, 589–611, 1997.

Moore, C. J.: Frequency-Response Corrections for Eddy-Correlation Systems, Boundary-Layer Meteorology, 37, 17–35, 1986.

Nemitz, E., Mammarella, I., Ibrom, A., Aurela, M., Burba, G., Dengel, S., Gielen, B., Grelle, A., Heinesch, B., Herbst, M., Hörtnagl, L., Klemedtsson, L., Lindroth, A., Lohila, A., McDermitt, D., Meier, P., Merbold, L., Nelson, D., Nicolini, G., Nilsson, M., Peltola, O., Rinne, J., and Zahniser, M.: Standardisation of eddy-covariance flux measurements of methane and nitrous oxide, International Agrophysics, 32, https://doi.org/10.1515/intag-2017-0042, 2018.

Nordbo, A., Kekäläinen, P., Siivola, E., Lehto, R., Vesala, T., and Timonen, J.: Tube transport of water vapor with condensation and desorption, Applied Physics Letters, 102, 194 101, https://doi.org/10.1063/1.4804639, 2013.

Nordbo, A., Kekäläinen, P., Siivola, E., Mammarella, I., Timonen, J., and Vesala, T.: Sorption-Caused Attenuation and Delay of Water Vapor Signals in Eddy-Covariance Sampling Tubes and Filters, Journal of Atmospheric and Oceanic Technology, 31, 2629–2649, https://doi.org/10.1175/JTECH-D-14-00056.1, https://doi.org/10.1175/JTECH-D-14-00056.1, 2014.

Peltola, O., Mammarella, I., Haapanala, S., Burba, G., and Vesala, T.: Field intercomparison of four methane gas analyzers suitable for eddy covariance flux measurements, Biogeosciences, 10, 3749–3765, https://doi.org/10.5194/bg-10-3749-2013, 2013.

Rannik, and Vesala, T.: Autoregressive filtering versus linear detrending in estimation of fluxes by the eddy covariance method, Boundary-Layer Meteorology, 91, 259–280, 1999.

Rannik, , Peltola, O., and Mammarella, I.: Random uncertainties of flux measurements by the eddy covariance technique, Atmospheric Measurement Techniques, 9, 5163–5181, https://doi.org/10.5194/amt-9-5163-2016, 2016.

Rebmann, C., Aubinet, M., Schmid, H., Arriga, N., Aurela, M., Burba, G., Clement, R., De Ligne, A., Fratini, G., Gielen, B., Grace, J., Graf, A., Gross, P., Haapanala, S., Herbst, M., Hörtnagl, L., Ibrom, A., Joly, L., Kljun, N., Kolle, O., Kowalski, A., Lindroth, A., Loustau, D., Mammarella, I., Mauder, M., Merbold, L., Metzger, S., Mölder, M., Montagnani, L., Papale, D., Pavelka, M., Peichl, M., Roland, M.,

Serrano-Ortiz, P., Siebicke, L., Steinbrecher, R., Tuovinen, J.-P., Vesala, T., Wohlfahrt, G., and Franz, D.: ICOS eddy covariance flux-station site setup: a review, International Agrophysics, 32, 471–494, https://doi.org/10.1515/intag-2017-0044, http://dx.doi.org/10.1515/intag-2017-0044, 2018.

Rinne, J., Tuittila, E.-S., Peltola, O., Li, X., Raivonen, M., Alekseychik, P., Haapanala, S., Pihlatie, M., Aurela, M., Mammarella, I., and Vesala, T.: Temporal Variation of Ecosystem Scale Methane Emission From a Boreal Fen in Relation to Temperature, Water Table Position, and Carbon Dioxide Fluxes, Global Biogeochemical Cycles, 32, 1087–1106, https://doi.org/10.1029/2017GB005747, https://doi.org/10.1029/2017GB005747, 2018.

Riutta, T., Laine, J., Aurela, M., Rinne, J., Vesala, T., Laurila, T., Haapanala, S., Pihlatie, M., and Tuittila, E. S.: Spatial variation in plant community functions regulates carbon gas dynamics in a boreal fen ecosystem, Tellus Series B-Chemical and Physical Meteorology, 59, 838–852, https://doi.org/10.1111/j.1600-0889.2007.00302.x, 2007.

Runkle, B. R. K., Wille, C., Gazovic, M., and Kutzbach, L.: Attenuation Correction Procedures for Water Vapour Fluxes from Closed-Path Eddy-Covariance Systems, Boundary-Layer Meteorology, 142, 401–423, https://doi.org/10.1007/s10546-011-9689-y, 2012.

Sabbatini, S., Mammarella, I., Arriga, N., Fratini, G., Graf, A., Hörtnagl, L., Ibrom, A., Longdoz, B., Mauder, M., Merbold, L., Metzger, S., Montagnani, L., Pitacco, A., Rebmann, C., Sedlák, P., Šigut, L., Vitale, D., and Papale, D.: Eddy covariance raw data processing for CO2 and energy fluxes calculation at ICOS ecosystem stations, International Agrophysics, 32, 495–515, https://doi.org/10.1515/intag-2017-0043, http://dx.doi.org/10.1515/intag-2017-0043, 2018.

Starkenburg, D., Metzger, S., Fochesatto, G. J., Alfieri, J. G., Gens, R., Prakash, A., and Cristóbal, J.: Assessment of Despiking Methods for Turbulence Data in Micrometeorology, Journal of Atmospheric and Oceanic Technology, 33, 2001–2013, https://doi.org/doi:10.1175/JTECH-D-15-0154.1, http://journals.ametsoc.org/doi/abs/10.1175/JTECH-D-15-0154.1, 2016.

Taipale, R., Ruuskanen, T. M., and Rinne, J.: Lag time determination in DEC measurements with PTR-MS, Atmos. Meas. Tech., 3, 853–862, https://doi.org/10.5194/amt-3-853-2010, https://amt.copernicus.org/articles/3/853/2010/https://amt.copernicus.org/articles/3/853/2010/amt-3-853-2010.pdf, 2010.

Vesala, T., Kljun, N., Rannik, , Rinne, J., Sogachev, A., Markkanen, T., Sabelfeld, K., Foken, T., and Leclerc, M. Y.: Flux and concentration footprint modelling: State of the art, Environmental Pollution, 152, 653–666, https://doi.org/http://dx.doi.org/10.1016/j.envpol.2007.06.070, http://www.sciencedirect.com/science/article/pii/S0269749107003399, 2008.

Wintjen, P., Ammann, C., Schrader, F., and Brümmer, C.: Correcting high-frequency losses of reactive nitrogen flux measurements, Atmos. Meas. Tech., 13, 2923–2948, https://doi.org/10.5194/amt-13-2923-2020, https://www.atmos-meas-tech.net/13/2923/2020/https://www.atmos-meas-tech.net/13/2923/2020/amt-13-2923-2020.pdf, 2020.